BRAIN COMMUNICATIONS

Lysosomal dysfunction impairs mitochondrial quality control and is associated with neurodegeneration in *TBCK* encephaloneuronopathy

Jesus A. Tintos-Hernández,[1] Adrian Santana,[1] Kierstin N. Keller[2] and Xilma R. Ortiz-González[1,3]

Biallelic variants in the *TBCK* gene cause intellectual disability with remarkable clinical variability, ranging from static encephalopathy to progressive neurodegeneration (TBCK-Encephaloneuronopathy). The biological factors underlying variable disease penetrance remain unknown. Since previous studies had suggested aberrant autophagy, we tested whether mitophagy and mitochondrial function are altered in *TBCK*$^{-/-}$ fibroblasts derived from patients exhibiting variable clinical severity. Our data show significant accumulation of mitophagosomes, reduced mitochondrial respiratory capacity and mitochondrial DNA content, suggesting impaired mitochondrial quality control. Furthermore, the degree of mitochondrial dysfunction correlates with a neurodegenerative clinical course. Since mitophagy ultimately depends on lysosomal degradation, we also examined lysosomal function. Our data show that lysosomal proteolytic function is significantly reduced in *TBCK*$^{-/-}$ fibroblasts. Moreover, acidifying lysosomal nanoparticles rescue the mitochondrial respiratory defects in fibroblasts, suggesting impaired mitochondrial quality control secondary to lysosomal dysfunction. Our data provide insight into the disease mechanisms of TBCK Encephaloneuronopathy and the potential relevance of mitochondrial function as a biomarker beyond primary mitochondrial disorders. It also supports the benefit of lysosomal acidification strategies for disorders of impaired lysosomal degradation affecting mitochondrial quality control.

1 Division of Neurology and Center for Mitochondrial and Epigenomic Medicine, The Children's Hospital of Philadelphia, Philadelphia, PA, USA
2 Department of Genetics, Center for Mitochondrial and Epigenomic Medicine, The Children's Hospital of Philadelphia, Philadelphia, PA, USA
3 Epilepsy Neurogenetics Initiative and Department of Neurology, Perelman School of Medicine, University of Pennsylvania, Philadelphia, PA 19104, USA

Correspondence to: Xilma R. Ortiz-González, MD, PhD,
Assistant Professor of Neurology and Pediatrics, University of Pennsylvania Pereleman School of Medicine, Division of Neurology, The Children's Hospital of Philadelphia, 3501 Civic Center Blvd, Philadelphia, PA 19104, USA
E-mail: ortizgonzalez@chop.edu

Keywords: mitochondria; mitophagy; neurodegeneration; intellectual disability; lysosome

Abbreviations: mtDNA = mitochondrial DNA; TBCK = TBC1-domain containing kinase; TBCKE = TBCK encephaloneuronopathy

Received August 03, 2020. Revised June 02, 2021. Accepted June 07, 2021. Advance Access publication September 16, 2021

Graphical Abstract

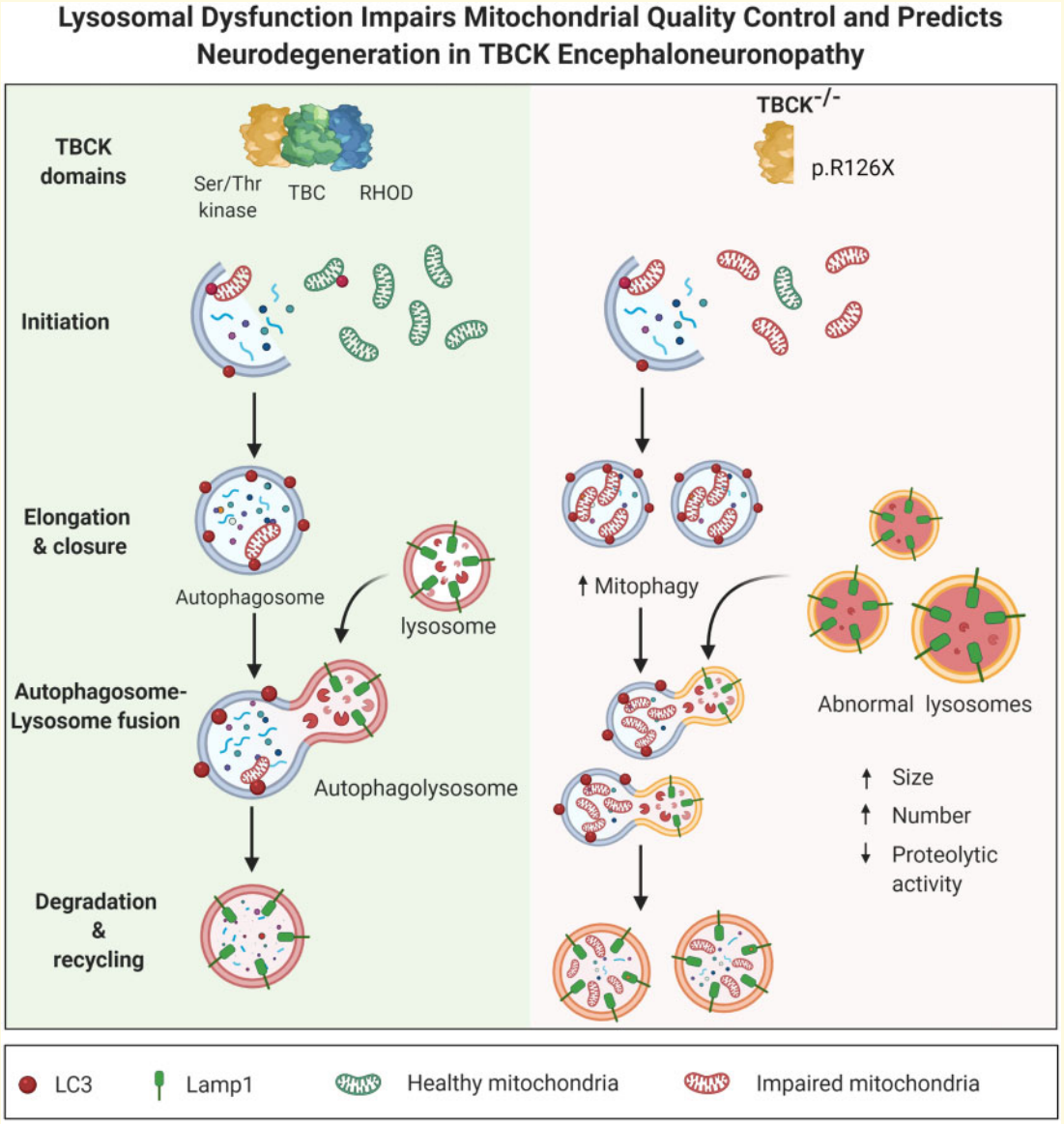

Introduction

Genetic variants causing mitochondrial and lysosomal disorders often present clinically with childhood-onset neurodegeneration. Considering the broader spectrum of common neurologic disorders, defects in these critical organelles have also been increasingly implicated in the pathogenesis of common neurodegenerative disorders like Parkinson's and Huntington's disease.[1–4] We have previously reported that biallelic mutations in the *TBCK* gene cause intellectual disability of variable severity in children (MIM: 616900), with some patients presenting with intellectual disability with autistic features and mild motor delays while others have profound delays and progressive encephalopathy.[5] We have further characterized a cohort of children of Puerto Rican descent sharing a *TBCK* truncating 'Boricua' mutation (p.R126X) who exhibit a severe neurodegenerative phenotype with prominent motor neuron degeneration, which we called TBCK-Encephaloneuronopathy (TBCKE).[6] How loss of function of TBCK protein leads to disease remains unclear, but patients exhibit clinical features reminiscent of lysosomal storage disorders (LSDs), including progressively coarse facies and macroglossia. Interestingly, other symptoms overlap with mitochondrial disease, such as metabolic strokes and neurologic decompensations with febrile illness.

TBCK encodes a protein of unclear function, TBC1-domain containing Kinase. It consists of a TBC (Tre-2, Bub2 and Cdc16) domain flanked by an N-terminal kinase-like domain and a rhodanese homology domain at the C-terminus. TBCK mRNA and protein appear to be expressed in most tissues of the human body.[7] Mouse brain transcriptome data show that TBCK is expressed in

astrocytes, neurons and oligodendrocytes.[8] Based on sequence homology with other TBC1-domain proteins, TBCK is predicted to function as a Rab GTPase-activating protein. Rab GTPases are key regulators of membrane trafficking.[9] Defects in Rab proteins and/or Rab GTPases leading to altered membrane trafficking have also been linked to common neurodegenerative disorders.[9,10] These proteins are thought to be particularly critical for neuronal health because trafficking and maturation of endosomes, autophagosomes and lysosomes are crucial for successful degradation of senescent proteins and organelles.[11,12] Furthermore, a critical developmental role of TBC1-domain containing family of Rab GTPases is recently emerging. In addition to TBCK, loss of function variants in genes encoding some of these proteins are associated with neurodevelopmental and intellectual disability syndromes, such as TBC1D24, TBC1D7, TBC1D20 and TBC1D23.

Previous *in vitro* studies suggest that *TBCK* knockdown lead to downregulation of mTOR (mechanistic target of rapamycin) signalling.[13,14] The mTOR pathway regulates crucial cellular responses, including growth, apoptosis, autophagy, translation, energy metabolism and inflammation.[15] The mTOR protein is a kinase that interacts with several proteins to form two distinct complexes named mTOR complex 1 (mTORC1) and mTOR complex 2 (mTORC2). Patient-derived TBCK-deficient cells showed a 78% decrease in phospho-ribosomal S6 phosphorylation (PS6), a widely used marker for mTORC1 downstream signalling.[16] The mTOR pathway is known to regulate autophagy, the physiologic process by which proteins, lipids and organelles are trafficked to lysosomes for degradation.[2,17] We previously examined autophagic function in TBCKE (i.e. severely affected neurodegenerative phenotype) and found increased autophagosomes and autophagic flux in TBCKE patient-derived fibroblasts.[6] Impaired autophagic-lysosomal function was also evident in aberrant oligosaccharide degradation profiles in TBCKE fibroblasts and was ameliorated by treating cells with L-leucine, a known mTORC1 signalling activator.[6]

Given these data, the first goal of this study was to examine if selective autophagy of mitochondria (mitophagy) is altered in TBCK-deficient cells. Defects in mitophagy have been linked to neurodegenerative disorders, most prominently Parkinson's disease.[18,19] Mitophagy is known to be induced by mTORC1 inhibition[20] as well as by disruption of lysosomal acidification.[21] In this study, we examined mitophagy as well as mitochondrial function for the first time in TBCK-deficient cells. In particular, this study asked if mitochondrial function varies in patients of diverging clinical severity.

Recent neuropathological reports have suggested a lysosomal storage-like phenotype in TBCK patients,[22,23] with pathological findings reminiscent of neuronal ceroid lipofuscinosis. As effective mitophagy is ultimately dependent on lysosomal degradation, we also examined lysosomal proteolytic activity in TBCK-deficient cells.

Taken together, our studies suggest that lysosomal dysfunction may contribute to impaired mitochondrial quality control and secondary mitochondrial dysfunction in TBCKE syndrome. This is the first report we are aware of outside of the primary mitochondrial depletion disorders, where mtDNA copy number and mitochondrial function correlate with severity of disease. Defective lysosomal degradation may constitute a final common pathway to explain a blockage in degradation of autophagosomes, mitophagosomes, as well as mediate the previously observed mTORC1 signalling inhibition in TBCKE. We also for the first time show that acidifying nanoparticles may have therapeutic benefit in disorders where effective mitophagy is disrupted.

Materials and methods

Cell culture

Primary patient fibroblasts were obtained with appropriate consent under an IRB-approved protocol at the Children's Hospital of Philadelphia. Fibroblasts were maintained in DMEM with glutamax media supplemented with 10–15% foetal bovine serum (FBS) and non-essential amino acids (NEAA). Experiments were carried out with cells of comparable passage number, and cells were not used past passage 15. Fibroblast lines derived from patients homozygous for the Boricua mutation (p.R126X), with a clinical course of progressive encephalopathy and motor neuronopathy are defined as 'severe' ($n = 4$ individual lines from unrelated patients, 126-1, 126-2, 126-3, 126-5). None of the p. R126X patients achieved language or independent ambulation. The 'mild' phenotype lines are derived from 3 patients with no clinical evidence of neurodegeneration. Two of the patients are siblings with global developmental delay but achieving expressive language and independently ambulation (although delayed, around age 2–3 yo, previously reported by Bhoj et al.). 'Mild' patients genotypes are as follows: lines 2685 and 2686 are compound heterozygous for a splice site and a frameshift variant (c.[2060-2A>G]; [803_806delTGAA], p.[=];[Met268fsArg*26]) and line 16-3607 is homozygous for exon 21 deletion. Control fibroblast cell lines (similar age individuals) were obtained from the NIGMS Human Genetic Cell Repository at the Coriell Institute for Medical Research: GM17064, GM17071 and GM08398B.

Mitochondrial assays

Mitophagy was assayed by live confocal imaging of primary TBCKE fibroblasts at basal culture conditions. Cells were plated in glass bottom 35 mm dishes (MatTek) and incubated with Mitotracker Green (ThermoFisher M7514) 25 nM for 15 min and Lysotracker Red (thermofisher) 50 nM for 25 min, and washed with pre-warmed

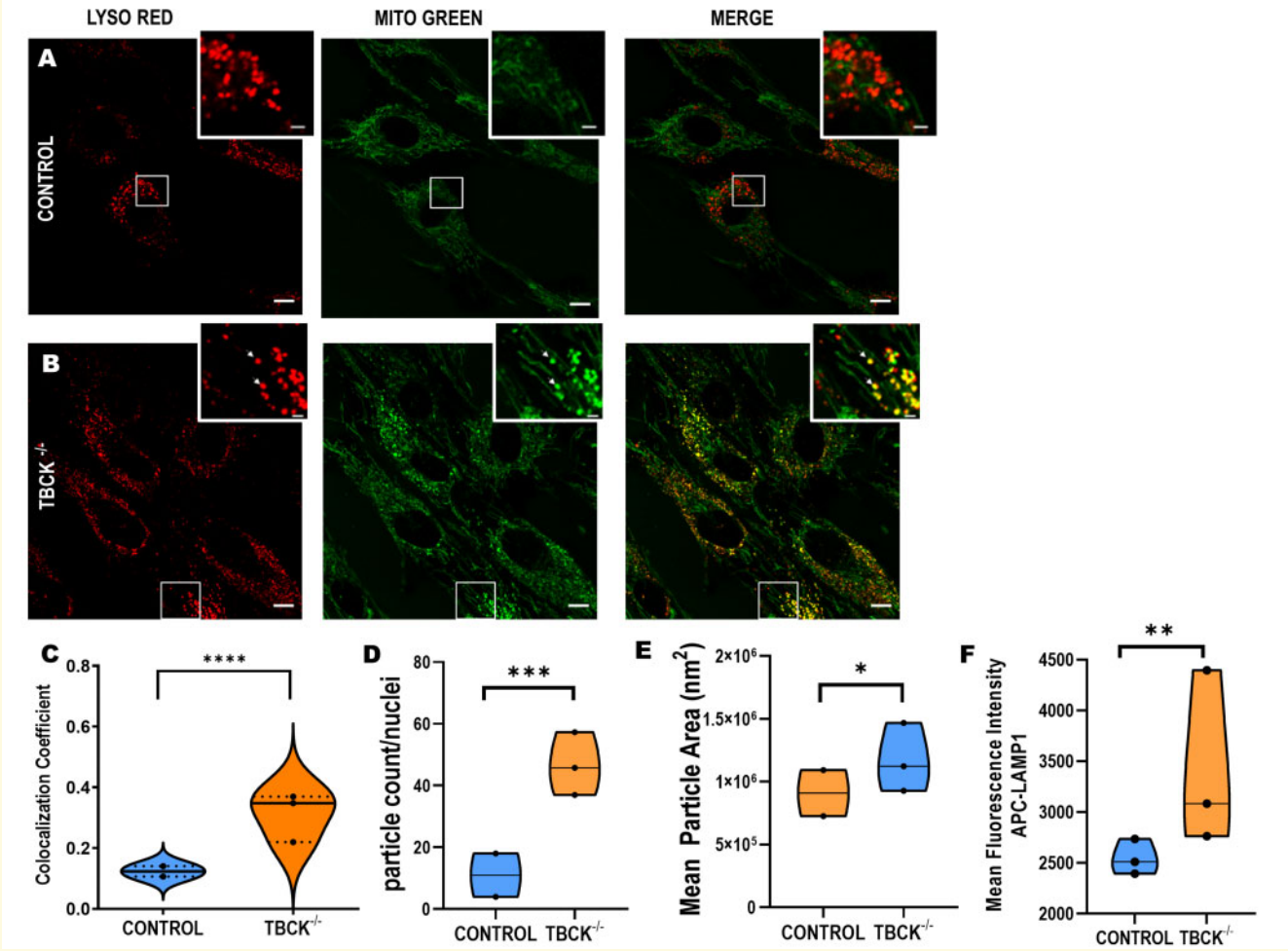

Figure 1 Mitophagy is upregulated in TBCKE fibroblasts. Confocal live imaging of human fibroblasts at baseline culture conditions, stained with Lysotracker red and Mitotracker green. Control (**a**) versus TBCKE (p.R126X) fibroblasts (**b**) are shown. TBCKE cells exhibit robust colocalization, a marker of mitophagy, scale bars =10 μm, inset 2 μm. Weighted colocalization coefficient (**c**) means plotted for fibroblast lines [2 controls, 3 TBCK p. R126X lines, Two-way ANOVA, $F(1,85) = 33.72$, $P < 0.0001$). Lysosomal content (**d**) was significantly increased, quantified as lysostracker positive particles per cell (nuclei) in live confocal images. Data obtained from in 3 independent experiments, analysed 2 plates per cell line, $n \geq 8$ images per line analysed using ZenBlue (controls = 0969, 2037; TBCK = 126-2, 126-3, 126-5). Mean lysotracker positive particle area per cell line plotted [two-way ANOVA $F(1,45) = 14.48$, $P = 0.004$). Analysing the lysotracker positive mean particle size using the same images is shown in **e**. Lysosomal size was significantly increased in TBCKE cells versus controls, Two-way ANOVA, $F(1,46) = 5.699$, $P = 0.0211$. LAMP1 immunostaining was also quantified as a marker of lysosomal content by flow cytometry (**f**), TBCKE cells had significantly increased LAMP1 mean fluorescence intensity compared to control cells $n = 2$ control lines and 3 TBCK lines, with 3 technical replicates per line [Two-way ANOVA, $F(1,11) = 18.54$, $P = 0.0012$).

PBS. Cells were imaged in an LSM710 (Carl Zeiss) confocal microscope equipped with temperature-controlled stage. Alternatively, to assay mitophagy by genetically encoded labels, fibroblasts were treated simultaneously with the LC3B-GFP (premo autophagy sensor Thermofisher P36235) and mito-RFP (thermofisher C10601) per manufacturer's instructions. For bafilomycin control experiments, cells were incubated in complete DMEM media containing 25 nM mitotracker green for 20 min at 37°C. Cells were then switched to complete media with 500 nM bafilomycin (4 h at 37°C). After treatment, media was exchanged with complete media together with 25 nM of lysotracker red (Thermofisher L7528) and ProLong® Live Antifade Reagent (Thermofisher P36975) and imaged as previously described.

Mitochondrial respiration

Baseline respiration and maximal respiratory capacity were measured using the Seahorse instrument (XF24 data for Figure 2 and Xe96 data for figures 3 and 5) according to the manufacturer's instructions (Agilent). Briefly, 20,000 cells were seeded per Xe96 plate well and cells were assayed within 24 h of plating unless otherwise noted. The following reagent concentrations were used:

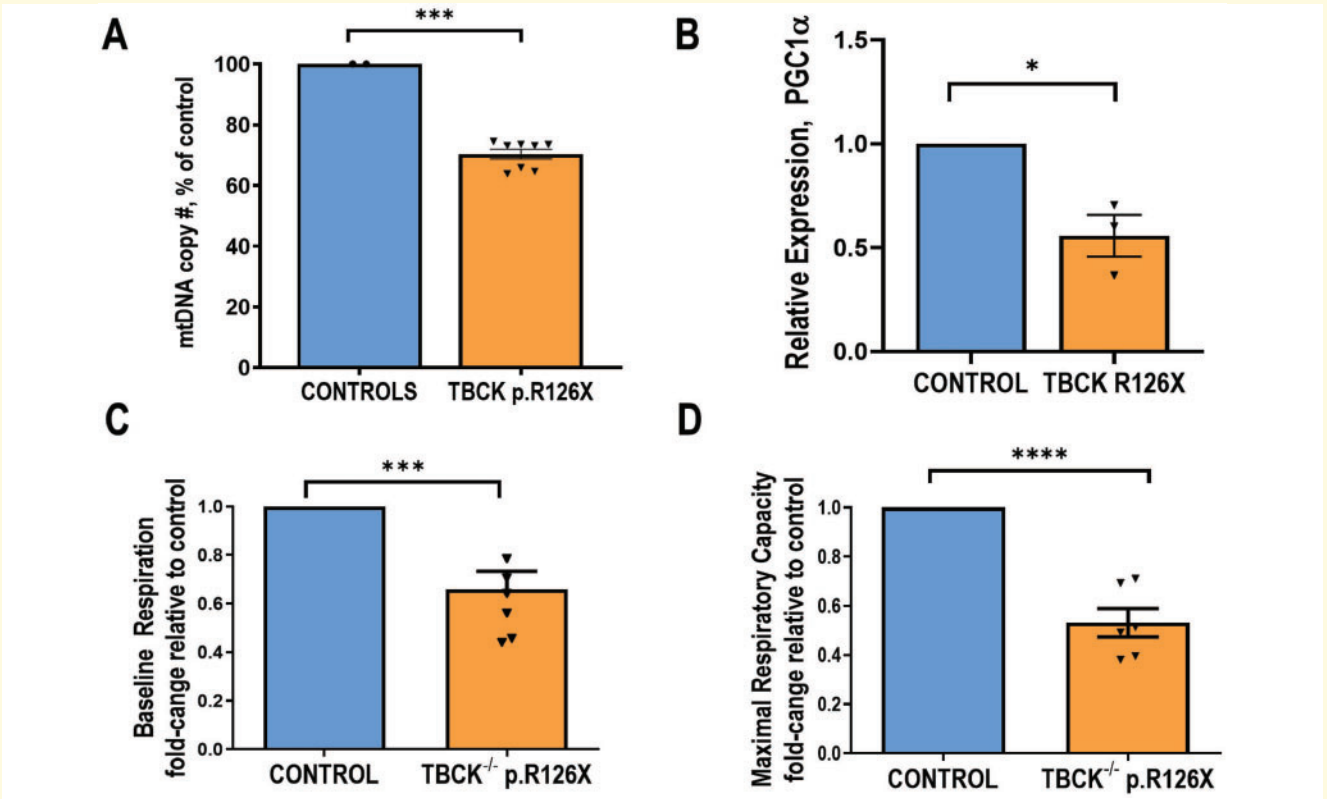

Figure 2 TBCKE fibroblasts have reduced mitochondrial DNA and respiratory function. mtDNA copy number (**a**) in four independent patient-derived lines homozygous for theTBCK Boricua variant (p.R126X, 126-1, 126-3, 126-5) normalized to controls ($n = 2$ lines) show nearly 30% reduction in mtDNA copy number, (mean 73.1%, SD ± 6.13 nested two-tailed *t*-test, $t_3 = 4.41$, $P = 0.0216$). (**b**) Expression of PGC1α, a key modulator of mitochondrial biogenesis is also decreased in TBCK$^{-/-}$ cells relative to controls (mean 0.55 SD ± 0.17, unpaired two-tailed $t_4 = 4.4$, $P = 0.0116$, mean of 3 different experiments plotted). Seahorse assays ($n \geq 4$ 96-well plate assays) of TBCK$^{-/-}$ fibroblasts (p.R126X) normalized to controls show (**c**) reduced baseline mitochondrial respiration (mean 0.66 SD ± 0.19, unpaired two-tailed *t*-test, $t_{12} = 4.56$, $P = 0.0007$) as well as (**d**) reduced FCCP stimulated maximal respiratory capacity (mean 0.53 SD ± 0.14 controls, unpaired two-tailed *t*-test, $t_{10} = 8.08$, $P < 0.0001$).

Oligomycin (1.25 μM), FCCP (1 μM), antimycin (1.8 μM) and rotenone (1 μM). For respiration assays with L-leucine treatment: Cells were plated as above but supplemented for 24 h with 600 μg/ml of L-leucine, as this dose was previously reported to augment mTORC1 mediated phosphorylation in TBCK$^{-/-}$ cells.[16]

Mitochondrial content

Mitochondrial mass was evaluated using anti-VDAC-1 staining quantified by flow cytometry. Briefly, cells were collected and washed with cold phosphate buffer saline (PBS), fixed with 4% PFH, and kept on FACS buffer (PBS, 0.5% BSA, 0.05% Sodium Azide). For staining cells were washed twice with Intracellular Staining Permeabilization Wash Buffer (Biolegend, Catalogue No. 421002), and re-suspended in same buffer with anti-VDAC-1 (1:200, abcam, Catalogue No. 15895) for 30 min at room temperature. Cell samples were washed with wash buffer and incubated secondary (Alexa Fluor® 647 Anti-Rabbit IgG Jackson Immuno Research Laboratories, Catalogue No. 111-605-003) for 30 at room temperature in the dark. After two washes with FACS buffer, cells were re-suspended on FACS buffer and assessed on CytoFLEX flow cytometer (Beckman Coulter, Life Science, Indianapolis, IN, USA). Flow data analysis was performed using FlowJo software.

Mitochondrial DNA copy number and gene expression assays

mtDNA copy number was assayed in fibroblasts from patients with TBCK mutations but distinct clinical phenotypes as described above. 'Mild' patients without evidence of disease progression ($n = 3$ fibroblast lines) were compared with the 'severe' Boricua p. R126X mutation ($n = 4$ fibroblast lines). Control lines were acquired commercially as detailed above. For mtDNA copy number, DNA was isolated using the manufacturer's protocol DNeasy Blood and tissue kit (QIAGEN, Catalogue No. 69506). Published primer sequences for CytB, ND4,

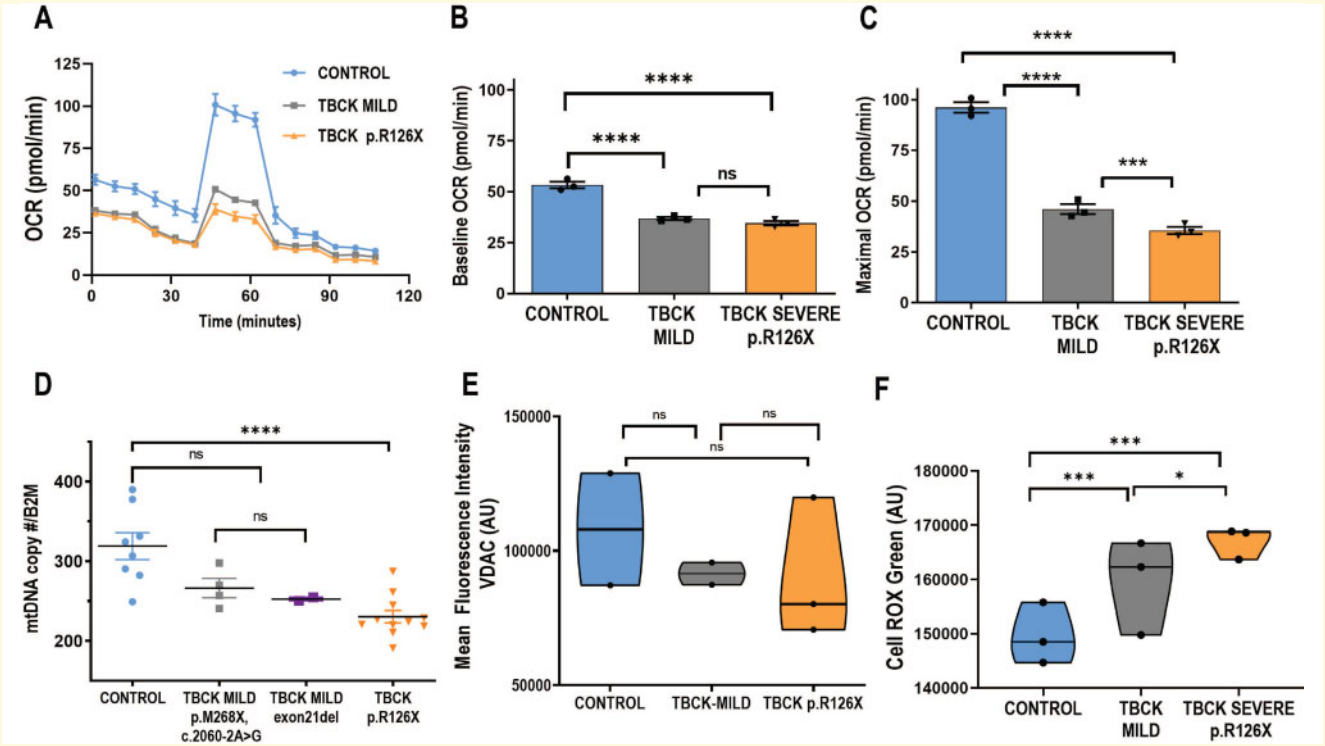

Figure 3 Reduced mitochondrial respiratory capacity and mtDNA correlate with severity of neurologic phenotype in TBCKE. Mitochondrial oxygen consumption rate (OCR) of control compared to *TBCK*$^{-/-}$ patient lines with mild (blue) versus severe (red) neurologic phenotypes. Both 'mild' and 'severe' groups included fibroblasts lines derived from at least 3 individual patients (see Supplementary Table 1 for details and genotypes). Panel **a** shows representative seahorse assay OCR tracing, plotted OCR values are mean ± SEM of minimum 10 wells per genotype. OCR values corresponding to mean for each cell line baseline respiration (**b**) and FCCP stimulated maximal respiratory capacity (**c**) are shown ($n = 3$ cell lines per genotype). Data analysed with two-way ANOVA with Tukey multiple comparisons test [For Baseline OCR $F(2,108) = 86.13$, $P < 0.0001$; for Maximal OCR $F(2,108) = 278.9$, $P < 0.0001$). mtDNA content (**d**), (normalized to nuclear gene *B2M*) also correlates with severity of neurologic phenotype, with mild TBCK patients exhibiting similar mtDNA copy number as controls while severe Boricua patients (p.R126X) have significantly decreased mtDNA copy number. Each qPCR sample was run in triplicate with $n > 2$ cell lines per genotype (except exon 21 del, only have 1 patient line available), in 2 independent experiments. Each value plotted represents mean of the technical triplicate for mtDNA copy number per cell line. Data analysed with one-way ANOVA with Dunnett's multiple comparison's test [$F(3,21) = 10.58$, $P = 0.0002$). Mitochondrial content per cell (**e**), assayed by immunostaining of mitochondrial outer membrane protein porin (VDAC) staining quantifed by flow cytometry, does not significantly differ in control versus TBCK$^{-/-}$ lines [One-way ANOVA, with Tukey's multiple comparison's test, $F(2,4) = 0.3766$, $P = 0.7082$] $n \geq 2$ cell lines per genotype, mean fluorescence intensity for VDAC was assayed in a minimum of 10 000 cells per sample, each cell line in duplicate. No significant difference found between groups (One-way ANOVA with Tukey's Multiple Comparisons test) Flow data analysed with FlowJo and plotted with Graphpad prism. Reactive oxygen species (ROS) elvels assayed by CellRox quantified by plate reader (**f**). $n = 3$ cell lines assayed per genotype, with 8 technical replicates each. Data analysed grouped per genotype, Two-way ANOVA with Tukey's multiple comparison's test [$F(2, 63) = 24.70$, $P < 0.0001$). Control versus Mild TBCK, $P = 0.0005$, Control versus TBCK severe $P < 0.0001$, TBCK mild versus TBCK severe $P = 0.0106$.

ND1, tRNA Leu (UUR), HRPT, B2M, 18s were used.[24,25]

For gene expression experiments, extraction of total RNA was performed using Rneasy Plus Universal mini kit (QIAGEN, Catalogue No. 73404), total RNA samples were processed with TURBO DNA-free™ Kit (ThermoFisher Scientific Inc., Catalogue No. AM1907) (1U/1μg RNA), for 30 min at 37°C, in order to avoid contaminant genomic DNA. Then, reverse transcription was performed using the SuperScript™ IV Reverse Transcriptase kit (ThermoFisher, Catalogue No. 18090010), with Oligo(dT)20 primer. For each cDNA sample, qPCR was performed with the following amplification primers: PGC1α (5′- TCC TCT TCA AGA TCC TGC TAT T3′; antisense, 5′ ACG GCT GTA GGG CGA TCT 3′). Stably expressed reference gene, GAPDH (sense, 5′ TCG GAG TCA ACG GAT TTG G 3′; antisense, 5′ TCG CCC CAC TTG ATT TTG GA 3′), was used for target gene expression normalization.

Amplifications were carried out in 384-well plates on VIIA7 thermocycler and each sample was analysed in triplicate. Negative controls without template were run for each gene. The reaction solution was prepared by combining 30 ng of DNA to each well as the template, 1× SYBR Green PCR Master Mix (Applied Bio systems)

and 0.4 mM of each of primer for a total volume of 10 μl. Amplification program: 10 min at 95°C, followed by 40 cycles of 15 s at 95°C and 60 s at 60°C. At the end of the amplification process, the melting curve was performed to assess amplification specificity of each gene. The corresponding real-time PCR efficiencies for each mitochondrial and nuclear gene amplification were calculated according to the equation: $E = 10(-1/\text{slope})-1$. Relative mtDNA copy number (mtDNA amount/nDNA amount) and relative expression levels of PGC1α were calculated by a comparative Ct method.

Lysosomal content and function assays

Lysosomal content: Lysotracker red puncta number and size per cell were analysed from confocal live imaging experiments from fibroblast as described above. LAMP1 staining was also quantified by flow cytometry as follows: Fibroblasts were harvested, permeabilized and stained with primary anti-LAMP1 antibody (1:50, H4A3 from DSHB, University of Iowa) and anti-mouse Alexa 647 antibody (Thermofisher). Blank and secondary only controls were used for each cell line. Mean fluorescence intensity (APC) was quantified using flow cytometry (CytoFLEX) and data analysed with FlowJo.

Proteolytic activity assays: Cathepsin D: Freshly isolated fibroblasts lysates were used to measure cathepsin D activity using a fluorometric plate reader assay per manufacturer's instructions (Abcam ab65302) For DQ-BSA assays: Fibroblasts were incubated for 4 h at 37°C with 10 µg/ml DQ^{TM} Green BSA (ThermoFisher, Catalogue No. D12050). Prior to staining cells were serum deprived for 4 h to maximize uptake. To further confirm live imaging findings and quantify proteolytic degradation, cells were also assayed by flow cytometry. Fibroblasts were treated with DQ-BSA versus blank controls and mean fluorescence intensity (FITC) was quantified using flow cytometry (CytoFLEX) and data analysed with FlowJo.

Neutral lipid staining was done with live fibroblasts treated with Bodipy D3922 1 µm for 30 min prior to live confocal imaging. For quantification, 10 000 cells per well were plated on 96-well plates. After 3 days in culture, cells were treated with 1 µM Bodipy for 30 min. After this incubation period, cells were washed 3 times with PBS. Fluorescence was measured in a microplate reader (493 nm excitation and 503 nm emission). Data were normalized to protein content per well.

Filipin staining: Fibroblasts were washed twice in PBS, fixed with 3% paraformaldehyde for 30 min at room temperature (RT) followed by 2 washes with PBS and incubated in quenching solution (1.5 mg/ml glycine, 1× PBS) at RT for 10 min. This was followed by incubating cells in 0.5 mg/ml filipin (ThermoFisher, Catalogue No. D3922), 10% FBS for 2 h at RT in the dark. After washing with PBS, cells were imaged using a Zeiss LSM 710 confocal microscope. For filipin quantification, 10 000 cells per well were plated on a 96 wells UV-transparent flat bottom plate (Corning 3635). Once confluent cells were washed, fixed and stain as described above for imaging. Samples were analysed immediately after staining with plate reader (360 nm excitation 430 nm emission). Data were normalized to protein content per well and mean fluorescence of a control line (8400) per plate.

Nanoparticles

Acidic nanoparticles (NPs) that have been previously shown effective in acidifying lysosomal pH and improving lysosomal function[26,27] weresynthesized by the Penn Nanoparticle Synthesis Core . Appropriate uptake into lysosomes in TBCK fibroblasts was verified by using Nile Red labelled NP and co-labeling with 50 nM lysotracker green (figure 5). NPs were resuspended in culture media (1 mg/ml), then sonicated for 10 min and filtered through a 0.8 µm filter (Corning, Catalog No. 431221). Fibroblasts were incubated in NP media for 3 days and then mitochondrial respiration was assayed using seahorse instrument as described above.

Live imaging assays

All live imaging experiments were performed in a Zeiss LSM 710 microscope with equipped with temperature-controlled stage. Cells were plated in 35 mm coverslip-bottom dishes with 14 mm glass diameter (MatTek). The same acquisition and analysis settings for all images within each experiment. FluoroBrite DMEM (ThermoFisher A1896701) media supplemented with 10% foetal bovine serum and GlutaMAX was utilized during imaging time. Weighted colocalization coefficient was determined using Zeiss Zen blue software using the same acquisition and analysis settings for all images. Mean particle area and particle counts per nuclei analysis was done with ZEN desk through Otsu's method for image segmentation.

Statistical analysis

All statistical analysis was performed using GraphPad Prism, with P-value <0.05 considered significant. For all figures, $^{*}P < 0.05$; $^{**}P < 0.01$, $^{***}P < 0.001$, $^{****}P < 0.0001$. Further details of experimental groups and statistical analysis for each experiment are provided in figure legends. At least 2 individual cell lines were used per genotype (control, TBCK severe, TBCK mild) unless otherwise noted. Experiments independently performed in at least triplicate, with representative data shown, unless specifically noted. For data shown in violin plots, solid line indicates the mean, while dotted line indicates quartiles. For each analysis, figure legends detail the experimental unit, the test statistic (e.g. t, U, F, r), degrees of freedom as subscripts to the test statistic [For ANOVA, F-values provided as F(DFn, DFd); for t-tests, $t_{DF.}$], and the exact probability value (P).

Data availability statement

The data that support the findings of this study are available from the corresponding author [XOG], upon reasonable request.

Results

TBCKE fibroblasts exhibit upregulation of mitophagy and reduced mtDNA content

We first tested whether mitophagy was altered in TBCK patient-derived versus control fibroblasts. Live confocal imaging shows extensive colocalization of functional mitochondrial and lysosomal markers, an indicator of mitophagy. Figure 1a shows representative images and the quantification of the colocalization coefficient in control versus TBCKE fibroblasts at baseline culture conditions ($n=2$ control lines and 2 TBCKE patient lines homozygous for p. R126X mutation). Interestingly, the level of colocalization indicative of mitophagosomes in TBCK cells, was an intermediate phenotype relative to control cells and controls treated with bafilomycin (Supplementary Fig. 1a and b). In order to confirm the upregulation of mitophagy with a different technique, we transduced control and TBCK fibroblasts with mito-RFP and LC3-GFP. We confirmed significant increase in colocalization coefficient relative to controls (Supplementary Fig. 1c and d) and observed mitochondria clearly enclosed in LC3-GFP positive autophagosomes in TBCK fibroblasts (Supplementary Fig. 1e).

Since we found evidence for upregulation of mitophagy, we then asked if mtDNA copy number was reduced in TBCKE fibroblasts, as mtDNA damage can be a trigger to initiate mitophagy.[28] Figure 2a shows that mtDNA copy number is significantly reduced in TBCKE fibroblasts from Boricua (p.R126X) mutation patients relative to controls. mtDNA copy number is not always directly correlate with mitochondrial mass, which is controlled by the interplay between mitochondrial biogenesis and degradation via mitophagy. mtDNA copy number per organelle is also dependent on availability of nucleotides for its synthesis (dNTPs), as well as replication machinery and stabilization (POLG, TFAM, etc.). In order to gain insight into whether less mtDNA in TBCK cells could be secondary to decreased generation of mitochondria, we assayed the expression of *PGC1α*, a transcription of co-activator that regulates mitochondrial biogenesis. We found that *PGC1α* expression was also significantly reduced in all TBCKE patient lines (Fig. 2b).

Given that TBCKE fibroblasts exhibit increased mitophagy and reduced mtDNA content, we then assayed mitochondrial respiratory capacity. Figure 2c and d shows that both baseline (c) and maximal respiratory capacity (d) are significantly reduced in TBCKE fibroblasts. Baseline respiratory capacity was 66% of controls, while maximal, FCCP (a mitochondrial uncoupler) stimulated respiratory capacity was 53% of control levels.

Mitochondrial dysfunction correlates with severity of clinical phenotype

We then asked whether mitochondrial function varies according to patient clinical severity. Mitochondrial respiratory capacity was measured in cell lines derived from patients with evidence of neurodegeneration ('severe' TBCKE patients, $n=4$ lines, all with the Boricua p. R126X homozygous mutation) and compared to cell lines from patients with a static clinical course ('mild', $n=3$ lines, see methods section for genotype details). Although all $TBCK^{-/-}$ patient lines exhibited significant mitochondrial respiration defects relative to controls (Fig. 3a and b), fibroblasts from severe Boricua patients had significantly lower maximal respiratory capacity than cells from mild patients (Fig. 3c). Interestingly, at baseline, mild versus severe phenotypes have similarly reduced oxygen consumption rates (Fig. 3b). This suggests that the severity of mitochondrial respiratory defects, specifically, the spare respiratory capacity, correlates with the severity of neurological deficits in patients with *TBCK* mutations.

To further examine the correlation of mitochondrial parameters with phenotype, we quantified mtDNA copy number in fibroblasts from severe versus mild patients, relative to healthy controls. Consistent with our respirometry data, mtDNA copy number was reduced in all TBCK patient lines, but most strikingly in the fibroblasts derived from the severely affected TBCKE patients with the Boricua mutation (mild 46% of control, severe 36% of control, Fig. 3d).

Reactive oxygen species levels, but not mitochondrial content, are significantly altered in TBCK cells

In order to understand why mtDNA content may be reduced in TBCK-deficient cells, we first examined whether there is reduced amount of mitochondria per cell. As a measure of mitochondrial content, we quantified the amount of VDAC-1 (porin), one of the most abundant outer membrane mitochondrial proteins which is encoded by nuclear DNA.[29] Multiple experiments quantifying porin by western blot and flow cytometry did not show significant decrease in mitochondrial content in $TBCK^{-/-}$ cells. Figure 3e shows flow cytometry quantification, despite a trend to lower mitochondrial content in TBCK affected cells, there was no statistically significant reduction in mitochondrial content per cell. Citrate synthase assays, another measure of mitochondrial content, also showed no significant differences between $TBCK^{-/-}$ and control lines (data not shown). If mtDNA copy number reduction is not due to reduced amount of

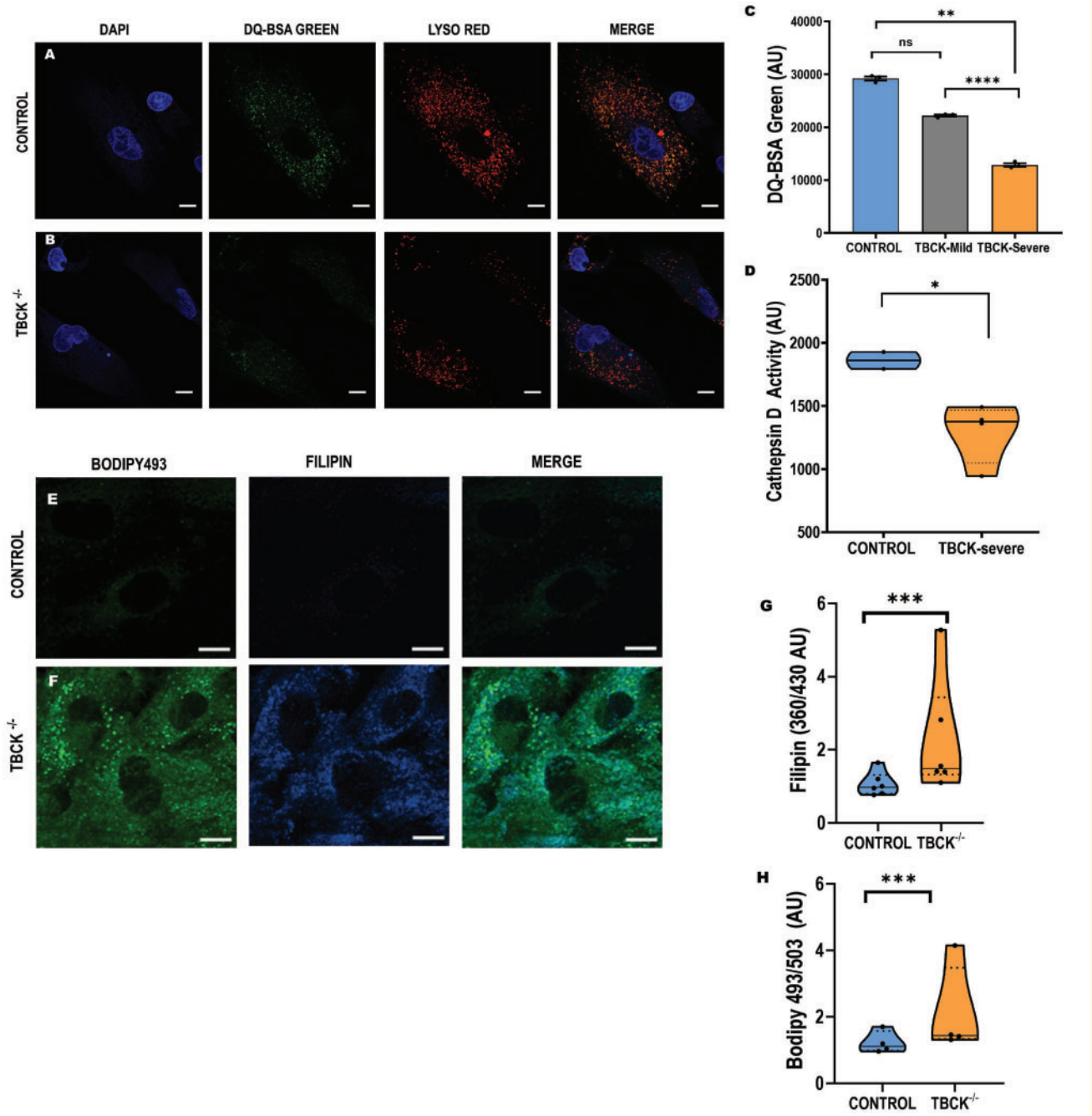

Figure 4 Lysosomal dysfunction in TBCKE fibroblasts. Lysosomal proteolytic activity visualized by live confocal imaging of DQ-BSA treated control (**a**) versus TBCK$^{-/-}$ (**b**) fibroblasts suggest reduced proteolytic activity in patient cells (decreased green DQ-BSA fluorescence and reduced colocalization with lysosomes in red). DQ-BSA fluorescence is dependent on lysosomal proteolytic cleavage. Panel **c** shows quantification of DQ-BSA by flow cytometry, Mean Fluorescence Intensity per cell line plotted for $n \geq 2$ cell lines per genotype (control, mild TBCK or severe TBCK). Each cell line assayed in triplicate and mean per cell line plotted [Two-way ANOVA with Tukey's Multiple Comparison tests, $F(2,4) = 6.357$; control versus mild TBCK non-significant, control versus severe TBCK $P = 0.0054$, Mild versus Severe TBCK $P < 0.0001$]. Panel **d** shows quantification of cathepsin D enzyme activity using a fluorometric plate reader assay in control versus TBCK p. R126X (severe); $n \geq 2$ independent cell lines per genotype (2 control lines and 4 TBCK lines), with each reaction ran in triplicate, mean per each cell line plotted [Two-way ANOVA, $F(1,20) = 7.578$, $P = 0.0123$]. Neutral lipid (BODIPY493), green, and filipin (cyan) costain in control (**e**) versus TBCK$^{-/-}$ (p.R126X, **f**) cells showing increased lipid droplets and unesterified cholesterol accumulation in TBCKE fibroblasts. Scale bar = 10 μm. Quantification by plate reader for both filipin (**g**) and BODIPY493 (**h**). For filipin data, $n = 2$ cell lines per genotype, per experiment, with 6 technical replicates per line per plate. Data were normalized to protein content per well and mean signal intensity of control line (8400) per plate. Data shown from 3 independent experiments (plates), mean per cell line plotted for each experiment [Two-way ANOVA $F(1,65) = 46.42$, $P < 0.0001$]. For Neutral lipid quantification of BODIPY, data shown is for 2 independent experiments with $n = 2$ control and 2 TBCK lines per experiment (6 technical replicates per line) assayed by plate reader. Absorbance 493/503 nm was normalized to protein content per well and then normalized to mean control line signal per plate, mean per cell line per experiment plotted [Two-way ANOVA $F(1,43) = 27.06$, $P < 0.001$].

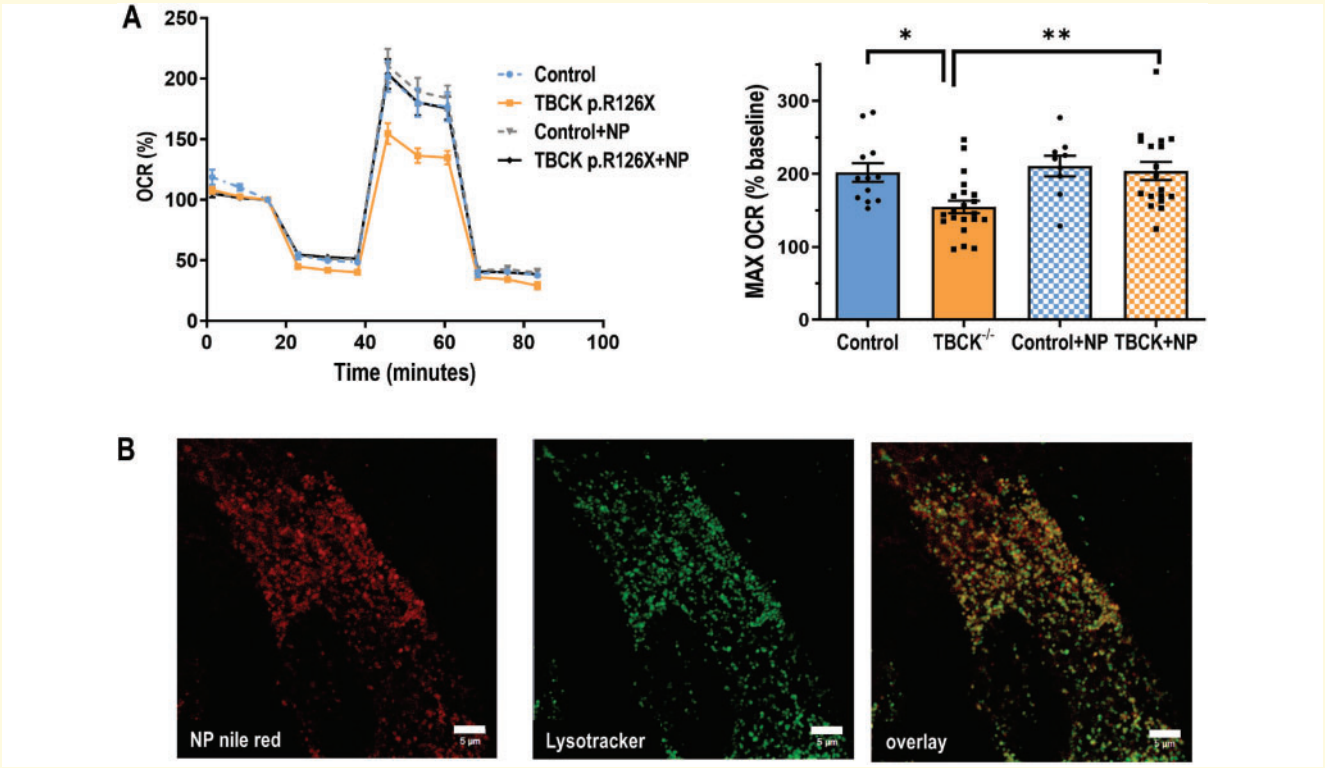

Figure 5 Lysosomal acidification rescues mitochondrial respiratory defects in TBCKE fibroblasts. Control and TBCK$^{-/-}$ fibroblasts were treated for 3 days with acidifying nanoparticles (NP, Penn nanoparticle core) and mitochondrial respiration assayed as previously using seahorse XF96 instrument. Mean oxygen consumption tracing as percent from baseline shown in **a** (left) for control lines ($n = 2$) versus TBCK fibroblasts ($n = 3$ lines). Each data point represents the mean OCR% for >4 wells per cell line and grouped per genotype. Right: Mean maximal OCR (as % of baseline, MAX OCR%) values for control lines showed no change in respiratory capacity after NP treatment, while maxOCR% in TBCK fibroblasts treated with NP was restored to control levels [One-way ANOVA with Tukey multiple comparisons test, $F(3,56) = 5.69$, $P = 0.0018$, for control versus TBCK $P = 0.0273$, for TBCK versus TBCK+NP $P = 0.0067$, control versus TBCK+NP $P = 0.99$]. Panel **b** shows control fibroblasts treated with nile-red nanoparticles (also from Penn nanoparticle core) colocalized with lysotracker green, verifying that NP are incorporated into the lysosomes (scale bar = 5 μm).

mitochondria per cell, an alternative scenario, since there are multiple copies of mtDNA per organelle, is reduced amount of mtDNA per mitochondria. Reactive oxygen species (ROS) generated in the mitochondria are known to induce mtDNA damage.[30] Therefore, we next assayed ROS levels at baseline conditions using CellROX in controls versus TCBK-deficient (mild and severe) fibroblasts. We found a striking increase of ROS levels in *TBCK*$^{-/-}$ cells, and furthermore, significant correlation with clinical severity (Fig. 3f). This observation is consistent with our mtDNA content data, and implicates that, concomitant with reduced *PGC1α* expression, elevated ROS levels may contribute to mtDNA depletion in TBCK.

TBCK-deficient fibroblasts have reduced lysosomal proteolytic activity

As mitophagy ultimately depends on lysosomal degradation, and increased mitophagosomes could be the result of a block in degradation, we assayed lysosomal proteolytic activity in TBCK-deficient fibroblasts. TBCK$^{-/-}$ fibroblasts had a moderate but significant decrease in enzymatic activity of the lysosomal protease cathepsin D (27% reduction, $n = 2$ control lines and $n = 4$ severe lines, Fig. 4a). To further examine lysosomal proteolytic function in fibroblasts, we treated cells with DQ-BSA. Fluorescence of this molecule is quenched at baseline, but activated once proteolytic degradation occurs within the acidic lysosome. We found by confocal imaging that DQ-BSA signal was visibly reduced in TBCKE fibroblasts (Fig. 4b), which was confirmed and quantified using flow cytometry (Fig. 4c). Fibroblasts derived from severe TBCKE Boricua patients had a significant 35% reduction in DQ-BSA proteolytic degradation relative to controls ($n = 2$ cell lines per group). Furthermore, we observed the same trend as we saw when quantifying mitochondrial function; that is, a significant impairment in lysosomal proteolytic activity correlates with the severity of clinical phenotype. We also observed accumulation of lipid droplets (stained with BODIPY neutral lipid green) and

unesterified cholesterol (by filipin staining) in TBCK-deficient cells, suggestive of lysosomal dysfunction (Fig. 4d).

Acidifying lysosomal nanoparticles, but not mTOR activation with l-leucine, rescue mitochondrial respiratory dysfunction in TBCK fibroblasts

In order to further examine if the mitochondrial dysfunction observed in TBCK could be secondary to lysosomal pathology, we tested whether acidifying nanoparticles that are incorporated into the lysosomes[26] rescue the mitochondrial respiratory defects in TBCK-deficient cells. $TBCK^{-/-}$ and control fibroblasts were treated for 3 days with acidifying nanoparticles and mitochondrial respiration studies performed as previously described. We found that both mild and severe $TBCK^{-/-}$ fibroblasts lines improved their mitochondrial maximal respiratory capacity after nanoparticle treatment (Fig. 5a). Figure 5b shows colocalization of nile-red labelled nanoparticles with lysotracker green, in order to confirm appropriate trafficking of nanoparticles into the lysosomes. On the other hand, L-leucine treatment, which has been shown to positively modulate mTORC1 mediated phosphorylation in TBCK-deficient cells[16] did not rescue the mitochondrial respiratory defects (Supplementary Fig. 2).

Discussion

Although we have made great advances in identifying novel disease genes in the next generation sequencing era, understanding how genetic changes affect biologic function in order to provide more accurate prognosis, and ultimately, treatments, remain a major challenge in the neurogenetics clinic. This is particularly challenging for novel disease genes with highly variable neurologic outcomes, such as the neurodevelopmental syndrome associated with *TBCK* mutations. Most, if not all, patients share significant hypotonia and motor delays in infancy and early childhood. Some patients proceed to gain developmental skills such as independent ambulation and expressive language, and have no clinical evidence of neurodevelopmental regression. Most commonly though, children experience progressive neurologic decline with prominent brain atrophy on serial imaging and evidence of motor neuron degeneration, which ultimately can be fatal due to chronic respiratory insufficiency. Genotype–phenotype correlations are not completely clear cut, as severely affected patients usually have truncating mutations early in the protein, but some of the mild patients also have splice site mutations that prevent protein expression and lead to undetectable protein levels.[16] Previous reports predicted, using *in silico* modelling, that most disease causing variants could alter the GAP activity domain.[5] In this study, we examined primary fibroblasts from patients with biallelic mutations in *TBCK*. Our data suggest that secondary mitochondrial dysfunction and the degree of mtDNA depletion correlate with a neurodegenerative course. Although our sample size is limited given this is an ultra-rare disease, it is noteworthy that this is the first demonstration outside of a primary mitochondrial depletion disorder where mtDNA copy number has been shown to correlate with the severity of neurological phenotype.

The physiologic function of TBCK remains unclear. It is predicted to act as a RabGTPase, based on sequence homology. Unbiased screening methods to detect effectors of Rab GTPases have found TBCK to bind to Rab5 in *drosophila*[31,32] but to our knowledge there are no clear published data to confirm the function of TBCK or its binding partners of TBCK in mammalian cells.

Other TBC1-domain containing proteins have also been proposed to interact with Rab7 and play a role in regulating delivery of clathrin-coated vesicles to the lysosome.[33] Rab7a is known to regulate endosomal transport and late endosome–lysosome fusion, but recent data specifically suggest a role in regulating autophagosome biogenesis during mitophagy, also known as mitophagosome formation.[34,35] It has been shown that Rab7A phosphorylation via TBK1 promotes mitophagy via the pink-parkin pathway.[36] Rab7 GTP hydrolysis has also been implicated in regulating mitochondria–lysosomal contact sites, controlling mitochondrial fission.[37]

Since autophagic-lysosomal clearance is abnormal in severe TBCKE (Boricua mutation) cells, this study focuses on mitophagy specifically, the physiologic removal of mitochondria by the autophagic cellular machinery. Autophagic degradation of abnormal mitochondria via mitophagy is particularly relevant to postmitotic cells like neurons and has been linked to neurodegenerative disorders, such as Parkinson's disease.[38–41] Our data show increased number of mitophagosomes in TBCKE fibroblasts as well as mitochondrial respiratory defects.

Mitochondrial disorders as well as mtDNA depletion syndromes are known to cause childhood-onset neurodegeneration.[42] Given the variable clinical phenotype of TBCK patients, we tested if the degree of mitochondrial dysfunction may distinguish the static versus neurodegenerative clinical course in patients with biallelic *TBCK* mutations.

We found the severity of the mitochondrial respiration correlates with a more severe neurological phenotype (see Fig. 3). mtDNA copy number was only significantly decreased in severe patients with the Boricua mutation. Our data suggest there is no significant decrease in mitochondrial content but that there are reduced levels of mtDNA and reduced respiratory function. Interestingly, impaired lysosomal acidification in LSD models has also been shown to be associated with decreased mitochondrial respiration, lower mtDNA content and increased ROS.[43,44]

Lysosomal dysfunction could also explain our previous observations of increased autophagic flux. That is because autophagy, including mitophagy, ultimately relies on lysosomes for degradation of defective proteins and organelles.[2,17] Since we reported increased autophagosomes and impaired degradation of oligosaccharides in TBCKE fibroblasts,[6] neuropathological reports from deceased TBCK patients have proposed reclassifying TBCK as a LSD based on evidence of lysosomal storage pathology in human brains.[22]

Consistent with those reports, our data also suggest lysosomal involvement in TBCKE, with a moderate (around 30–35%) but statistically significant decrease in proteolytic lysosomal activity (assayed by cathepsin and DQ-BSA hydrolysis) when comparing severe $TBCK^{-/-}$ patient lines to controls (Fig. 4). Furthermore, the correlation with severity of phenotype is also maintained, with mild $TBCK^{-/-}$ lines showing 10–15% decrease in activity that is not statistically significantly different than controls (Fig. 4c). Not only we show evidence for lysosomal proteolytic defects in TBCK fibroblasts, we also show accumulation of lipid droplets and unesterified cholesterol, reminiscent of other LSD. Quantification of lysosomal content and size showed increased number lysosomes (labelled both by LAMP-1 and lysotracker red) and larger lysosome size in TBCKE cells (Fig. 1d–f). Although we did not examine lysosomal pH directly, we show that lysosomal acidification strategies rescue the mitochondrial respiratory defects in TBCKE cells (Fig. 5).

Overall, our data suggest that impairment in lysosomal function lead to impaired mitochondrial quality control, reduction of mtDNA and respiratory dysfunction. The severity of the mitochondrial impairment, which can be rescued with lysosomal acidification, predicts the neurodegenerative course in TBCK Encephaloneuronopathy. Our data suggesting lysosomal dysfunction may also provide a mechanistic link with the previous observation of decreased mTORC1 signalling. It has been shown that mTORC1 activation and sensing of amino acids occurs at the lysosomal surface, and previous studies have shown that lysosomal dysfunction is sufficient to inhibit mTORC1 signalling.[45,46] In our studies, mTOR modulation with L-leucine did not alter the mitochondrial dysfunction (Supplementary Fig. 2).

Further studies could address whether the increased number of mitophagosomes we observed could be due to TBCK leading to impaired Rab5 and/or Rab7 cycling, altering mitophagosome biogenesis and/or mitochondrial–lysosomal contacts. Future studies should also examine if lysosomal uptake and endosomal trafficking pathways are intact in TBCK, as this has been shown to play a role in some classic LSDs such as batten's disease due to CLN3 mutations.[47,48]

In conclusion, our findings suggest that cells from patients with severe TBCK Encephaloneuronopathy exhibit secondary mitochondrial dysfunction due to autophagolysosomal pathway dysfunction. Our data support the recent classification of TBCKE as a 'congenital disorders of autophagy'.[49] Our findings also suggest mechanistic overlap with LSDs, such as proteolytic degradation defects and lipid accumulation, consistent with a neuropathological lysosomal storage phenotype in TBCK patients.[22]

Supplementary material

Supplementary material is available at *Brain Communications* online.

Acknowledgements

First and foremost, we want to thank the patients and their families for their invaluable contribution to this research. We also thank our collaborators Dr Elizabeth Bhoj and Dr Daniel Doherty for referring patients to our cohort. Dr Claire Mitchell generously provided the nanoparticles for the pilot lysosomal rescue studies. Dr Douglas Wallace and the Center for Mitochondrial and Epigenomic Medicine for providing access to shared equipment and imaging facilities.

Funding

X.O.G. was supported by the Robert Wood Johnson Harold Amos Faculty Development Award; the Children's Hospital of Philadelphia Roberts Collaborative, and Foerderer Award; and National Institute of Neurological Disorders and Stroke (1K02NS112456-01A1).

Competing interests

The authors report no competing interests.

References

1. Wallace DC. Bioenergetic origins of complexity and disease. Cold Spring Harb Symp Quant Biol. 2011;76:1.
2. Menzies FM, Fleming A, Rubinsztein DC. Compromised autophagy and neurodegenerative diseases. Nat Rev Neurosci. 2015;16(6):345–357.
3. Whyte LS, Lau AA, Hemsley KM, Hopwood JJ, Sargeant TJ. Endo-lysosomal and autophagic dysfunction: A driving factor in Alzheimer's disease? J Neurochem. 2017;140(5):703–717.
4. Schon E, Przedborski S. Mitochondria: The next (neurode)generation. Neuron. 2011;70(6):1033–1053.
5. Chong JX, Caputo V, Phelps IG, et al. University of Washington Center for Mendelian Genomics. Recessive inactivating mutations in TBCK, encoding a Rab GTPase-activating protein, cause severe infantile syndromic encephalopathy. Am J Hum Genet. 2016;98(4):772–781.
6. Ortiz-Gonzalez XR, Tintos-Hernandez JA, Keller K, et al. Homozygous boricua TBCK mutation causes neurodegeneration and aberrant autophagy. Ann Neurol. 2018;83(1):153–165.
7. Uhlen M, Fagerberg L, Hallstrom BM, et al. Proteomics. Tissue-based map of the human proteome. Science. 2015;347(6220):1260419.

8. Zhang Y, Chen K, Sloan SA, et al. An RNA-sequencing transcriptome and splicing database of glia, neurons, and vascular cells of the cerebral cortex. J Neurosci. 2014;34(36):11929–11947.
9. Kiral FR, Kohrs FE, Jin EJ, Hiesinger PR. Rab GTPases and membrane trafficking in neurodegeneration. Curr Biol. 2018;28(8): R471–R486.
10. Shi MM, Shi CH, Xu YM. Rab GTPases: The key players in the molecular pathway of Parkinson's disease. Front Cell Neurosci. 2017;11:81.
11. Ao X, Zou L, Wu Y. Regulation of autophagy by the Rab GTPase network. Cell Death Differ. 2014;21(3):348–358.
12. Bento CF, Puri C, Moreau K, Rubinsztein DC. The role of membrane-trafficking small GTPases in the regulation of autophagy. J Cell Sci. 2013;126(Pt 5):1059–1069.
13. Liu Y, Yan X, Zhou T. TBCK influences cell proliferation, cell size and mTOR signaling pathway. PLoS One. 2013;8(8):e71349.
14. Wu J, Li Q, Li Y, et al. A long type of TBCK is a novel cytoplasmic and mitotic apparatus-associated protein likely suppressing cell proliferation. J Genet Genomics. 2014;41(2):69–72.
15. Laplante M, Sabatini DM. mTOR signaling in growth control and disease. Cell. 2012;149(2):274–293.
16. Bhoj EJ, Li D, Harr M, et al. Mutations in TBCK, encoding TBC1-domain-containing kinase, lead to a recognizable syndrome of intellectual disability and hypotonia. Am J Hum Genet. 2016; 98(4):782–788.
17. Tsukada M, Ohsumi Y. Isolation and characterization of autophagy-defective mutants of *Saccharomyces cerevisiae*. FEBS Lett. 1993;333(1-2):169–174.
18. Narendra D, Tanaka A, Suen DF, Youle RJ. Parkin is recruited selectively to impaired mitochondria and promotes their autophagy. J Cell Biol. 2008;183(5):795–803.
19. Narendra D, Tanaka A, Suen DF, Youle RJ. Parkin-induced mitophagy in the pathogenesis of Parkinson disease. Autophagy. 2009;5(5):706–708.
20. Pan T, Rawal P, Wu Y, Xie W, Jankovic J, Le W. Rapamycin protects against rotenone-induced apoptosis through autophagy induction. Neuroscience. 2009;164(2):541–551.
21. Ding WX, Yin XM. Mitophagy: Mechanisms, pathophysiological roles, and analysis. Biol Chem. 2012;393(7):547–564.
22. Beck-Wodl S, Harzer K, Sturm M, et al. Homozygous TBC1 domain-containing kinase (TBCK) mutation causes a novel lysosomal storage disease - A new type of neuronal ceroid lipofuscinosis (CLN15)? Acta Neuropathol Commun. 2018;6(1):145.
23. Sumathipala D, Stromme P, Gilissen C, Corominas J, Frengen E, Misceo D. TBCK encephaloneuropathy with abnormal lysosomal storage: Use of a structural variant bioinformatics pipeline on whole-genome sequencing data unravels a 20-year-old clinical mystery. Pediatr Neurol. 2019;96:74–75.
24. Venegas V, Halberg MC. Measurement of mitochondrial DNA copy number. Methods Mol Biol. 2012;837:327–335.
25. Kaaman M, Sparks LM, van Harmelen V, et al. Strong association between mitochondrial DNA copy number and lipogenesis in human white adipose tissue. Diabetologia. 2007;50(12): 2526–2533.
26. Baltazar GC, Guha S, Lu W, et al. Acidic nanoparticles are trafficked to lysosomes and restore an acidic lysosomal pH and degradative function to compromised ARPE-19 cells. PLoS One. 2012;7(12):e49635.
27. Lee JH, McBrayer MK, Wolfe DM, et al. Presenilin 1 maintains lysosomal Ca(2+) homeostasis via TRPML1 by regulating vATPase-mediated lysosome acidification. Cell Rep. 2015;12(9): 1430–1444.
28. Gilkerson RW, De Vries RL, Lebot P, et al. Mitochondrial autophagy in cells with mtDNA mutations results from synergistic loss of transmembrane potential and mTORC1 inhibition. Hum Mol Genet. 2012;21(5):978–990.
29. Janes MS, Hanson BJ, Hill DM, et al. Rapid analysis of mitochondrial DNA depletion by fluorescence in situ hybridization and immunocytochemistry: Potential strategies for HIV therapeutic monitoring. J Histochem Cytochem. 2004;52(8):1011–1018.
30. Nissanka N, Moraes CT. Mitochondrial DNA damage and reactive oxygen species in neurodegenerative disease. FEBS Lett. 2018; 592(5):728–742.
31. Gillingham AK, Bertram J, Begum F, Munro S. In vivo identification of GTPase interactors by mitochondrial relocalization and proximity biotinylation. Elife. 2019;8:8.
32. Gillingham AK, Sinka R, Torres IL, Lilley KS, Munro S. Toward a comprehensive map of the effectors of rab GTPases. Dev Cell. 2014;31(3):358–373.
33. Frasa MA, Koessmeier KT, Ahmadian MR, Braga VM. Illuminating the functional and structural repertoire of human TBC/RABGAPs. Nat Rev Mol Cell Biol. 2012;13(2):67–73.
34. Yamano K, Fogel AI, Wang C, van der Bliek AM, Youle RJ. Mitochondrial Rab GAPs govern autophagosome biogenesis during mitophagy. Elife. 2014;3:e01612.
35. Tan EHN, Tang BL. Rab7a and mitophagosome formation. Cells. 2019;8(3):224.
36. Heo JM, Ordureau A, Swarup S, et al. RAB7A phosphorylation by TBK1 promotes mitophagy via the PINK-PARKIN pathway. Sci Adv. 2018;4(11):eaav0443.
37. Wong YC, Ysselstein D, Krainc D. Mitochondria-lysosome contacts regulate mitochondrial fission via RAB7 GTP hydrolysis. Nature. 2018;554(7692):382–386.
38. Valente EM, Abou-Sleiman PM, Caputo V, et al. Hereditary early-onset Parkinson's disease caused by mutations in PINK1. Science. 2004;304(5674):1158–1160.
39. Valente EM, Salvi S, Ialongo T, et al. PINK1 mutations are associated with sporadic early-onset parkinsonism. Ann Neurol. 2004; 56(3):336–341.
40. Matsumine H, Saito M, Shimoda-Matsubayashi S, et al. Localization of a gene for an autosomal recessive form of juvenile Parkinsonism to chromosome 6q25.2-27. Am J Hum Genet. 1997; 60(3):588–596.
41. Kitada T, Asakawa S, Hattori N, et al. Mutations in the parkin gene cause autosomal recessive juvenile parkinsonism. Nature. 1998;392(6676):605–608.
42. Young MJ, Copeland WC. Human mitochondrial DNA replication machinery and disease. Curr Opin Genet Dev. 2016;38: 52–62.
43. Weber RA, Yen FS, Nicholson SPV, et al. Maintaining Iron Homeostasis Is the Key Role of Lysosomal Acidity for Cell Proliferation. Mol Cell. 2020;77(3):645–655 e7.
44. Yambire KF, Rostosky C, Watanabe T, et al. Impaired lysosomal acidification triggers iron deficiency and inflammation in vivo. Elife. 2019;8:e51031.
45. Li M, Khambu B, Zhang H, et al. Suppression of lysosome function induces autophagy via a feedback down-regulation of MTOR complex 1 (MTORC1) activity. J Biol Chem. Dec 13 2013; 288(50):35769–35780.
46. Bar-Peled L, Sabatini DM. Regulation of mTORC1 by amino acids. Trends Cell Biol. 2014;24(7):400–406.
47. Schultz ML, Tecedor L, Stein CS, Stamnes MA, Davidson BL. CLN3 deficient cells display defects in the ARF1-Cdc42 pathway and actin-dependent events. PLoS One. 2014;9(5):e96647.
48. Schultz ML, Tecedor L, Lysenko E, Ramachandran S, Stein CS, Davidson BL. Modulating membrane fluidity corrects Batten disease phenotypes in vitro and in vivo. Neurobiol Dis. 2018;115: 182–193.
49. Teinert J, Behne R, Wimmer M, Ebrahimi-Fakhari D. Novel insights into the clinical and molecular spectrum of congenital disorders of autophagy. J Inherit Metab Dis. 2020;43(1):51–62.